Journal of the European Ceramic Society 20 (2000) 1729–1737

Fine grained Mg–PSZ ceramics with titania and alumina or spinel additions for near net shape steel processing

C.G. Aneziris *, E.M. Pfaff, H.R. Maier

Institute for Ceramic Components in Mechanical Engineering, RWTH Aachen, Nizzaallee 32, 52072 Aachen, Germany

Received 29 September 1999; received in revised form 26 January 2000; accepted 2 February 2000

Abstract

Mg–PSZ materials exhibit high corrosion resistance in steel/slag-systems. Through special additions of TiO_2 and Al_2O_3 or $MgAl_2O_4$ special microstructures have been obtained by slip casting with improved thermal shock performance and corrosion resistance for applications in near net shape steel processing. The thermomechanical properties have been measured at room and at elevated temperatures up to 1450°C and the corrosion rates have been investigated in a specially designed device simulating real operating conditions of thin slab casting of steel. The thermal shock behaviour has been evaluated due to water quenching tests and measuring of the remaining four point bending strengths. In addition disc shapes have been shocked by the aid of an arc torch.

Zusammenfassung

Mg–PSZ Werkstoffe präsentieren sehr vorteilhafte Korrosionseigenschaften in Stahl-Schlacke-Systemen. Mit Hilfe von TiO_2-, Al_2O_3- oder $MgAl_2O_4$-Zusätzen sind spezielle Mikrogefüge mit verbesserten Thermoschock- und Korrosionseigenschaften für Anwendungen in endabmessungsnahen Stahlstranggießtechnologien erzeugt worden. Die thermischen und mechanischen Eigenschaften sind zwischen RT und 1450°C ermittelt worden, und die Korrosionsraten wurden in einer speziell konstruierten Versuchsanordnung, wo Betriebsbedingungen vom Dünnbrammenguß simuliert werden, erfaßt. Das Thermoschock-Verhalten wurde anhand von Restfestigkeiten von Proben, die vorher in Wasser abgeschreckt worden sind, untersucht. Zusätzlich wurden Plattengeometrien mit Hilfe einer Schweißbrennerflamme beansprucht.

Résumé

La Mg–PSZ montre avantageuse propriétés des materiaux réfractaires disponibles à l'usage de la système d'acier et slag. A l'aide des TiO_2-, Al_2O_3- ou $MgAl_2O_4$-additives les structures microscopiques spéciales avec la meilleure résistance à le thermochoc et la corrosion à l'usage de la technologie de la coulée continue d'acier à mesure exacte ont été produit. Les propriétés thermique et mécanique de 23°C à 1450°C ont été trouvé. Pour simuler des conditions de service un montage expérimental spécial a été construit. Avec celui-ci les taux de corrosion ont été sait. Le comportement thermique a été examiné avec le fermeté qui reste après passer à l'eau froide. Supplémentaire les géométries plates ont été soumettre à des éfforts avec le flamme du sueur.

Keywords: Corrosion resistance; Microstructure-final; Refractories; Steel processing; Thermal shock resistance; ZrO_2

1. Introduction

The phase equilibrium of zirconia with other oxide systems is fundamental to the application of zirconia as an advanced refractory ceramic. Of greatest interest are the oxides such as MgO or Y_2O_3 with similar atomic radii, which dissolve to a significant extent in zirconia and tend to stabilise, full or partially, the cubic fluorite phase.[1]

In the case of hot steel applications, such as the near net shape steel processing with its basic versions of thin slab casting and strip casting, low porous MgO partially stabilised ZrO_2 (Mg–PSZ) shows the highest corrosion resistance at the interphase steel/slag/ceramic, at the interphase slag/ceramic/ air and against steel and its

* Corresponding author.
E-mail address: ca@ikkm.rwth-aachen.de (C.G. Aneziris).

0955-2219/00/$ - see front matter
PII: S0955-2219(00)00050-9

alloys in comparison to all conventional oxide and non-oxide refractory materials.[2–4] As a competitor BN also appears with very good properties against corrosion attack at the above mentioned interphases, but unfortunately it partially dissolves in steel. Further, the manufacturing costs for a monolithic component (submerged nozzle or slide gate) are much higher in comparison to densed zirconia components.[5]

In spite of this excellent performance in aggressive corrosive environments, zirconia suffers under thermal shock attack. Especially in the secondary metallurgy, critical casting components such as nozzles have to survive the thermal shock attack in the beginning of casting when the molten steel of the tundish (1580°C) contacts the preheated ceramic. Due to insufficient preheating control during operation, a temperature difference up to 500°C has to be bridged. Hasselman has established the thermal stress resistance parameters related to the thermal expansion coefficient, the Young's modulus of elasticity, the fracture tensile stress and the thermal conductivity. He has illustrated the effect of thermal shock on the strength of ceramics and the regions of applicability (resistance to fracture, loss in strength due to fracture and crack stability followed by further weakening) of the various thermal stress fracture parameters.[6,7]

In order to control the microstructure for superior thermomechanical and corrosion resistance properties several scientists have worked with different stabilising agents and additives for zirconia based materials.[8,9] This paper concentrates on the influence of Al_2O_3, TiO_2 and $MgAl_2O_4$ additives in Mg–PSZ materials because of their contribution to thermal shock behaviour.[10]

In particular, the fracture toughness and fracture behaviour of ZrO_2–Al_2O_3-ceramics are influenced strongly by the size, size distribution and location of the particles.[11] Small additions of TiO_2 (0.5 mol%) are suggested as a sintering aid.[12] In the case of Y_2O_3 stabilised zirconia, additions of Al_2O_3 and TiO_2 have been induced due to a plasma powder preparing technique, where structures are consistent with co-condensation of the liquid phase to form ultrafine droplets and a variety of metastable phases during solidification.[13] Further, an increased TiO_2-content in Y_2O_3 stabilised ZrO_2 increases the grain size of zirconia and destabilises the cubic phase.[14] In the case of the cubic phase destabilisation the c-axis of the tetragonal structure increases while the a-axis decreases. This is quite interesting because the ionic radius of Ti^{4+} is smaller than that of Zr^{4+}. The destabilisation of the cubic phase is attributed to the reduced coordination number.[15] Besides this explanation an additional reason for this expansion of the c-axis and contraction of the a-axis with increasing TiO_2 content is believed to be due to the preferred repulsion between Ti^{4+} cations and the effective double positive charged oxygen vacancies in [001] direction. The length change in both directions suggests that the Ti^{4+} cations are not incorporated randomly in the lattice (up to 6.71 wt% TiO_2 a solid solution in zirconia is expected, $ZrTiO_4$ does not exist[16]) but in preferred energetically favourable sites which cause a repulsion between the dopant cations and the vacancies.[17] Furthermore there is a progressive decrease in the temperature of inversion (tetragonal to monoclinic) as the amount of TiO_2 is increased, lowering the point of the polymorphic change from about 980°C for pure ZrO_2 to about 340°C for specimens containing 40 mol% TiO_2.[18]

In general ZrO_2 with Ti (metal) additions exceeding the solubility limit (>4 mol%) showed better sintering due to liquid–phase sintering and had better strength and thermal shock resistance than ZrO_2 with less or no Ti. The improved thermal shock resistance could be attributed to the better thermal conductivity and plasticity of metallic Ti.[19,20] The presence of Ti in ZrO_2 during sintering inhibits the grain growth and the smaller grain size of ZrO_2 leads also to a better thermal shock performance.[21]

Another work describes fine grained Mg–PSZ-type that has been produced by adding $MgAl_2O_4$ spinel to a ternary Y_2O_3–MgO–ZrO_2 system. A mean cubic grain size below 10 μm has been achieved and through special aging treatment the toughness has been improved through the formation of transformable tetragonal precipitates.[22]

In many cases of partial MgO stabilised zirconias the tetragonal phase can be recognised as spheroids or lenses of approximately 50–500 nm in big cubic grains or at their grain boundaries, whereby the tetragonal "lenses" are aligned at right angles.[23,24] During thermal, chemical, mechanical or kinetical (particle size) destabilisation a martensitic phase transformation takes place (tetragonal to monoclinic).[25] Martensitic monoclinic twins appear in the cubic crystal (or at the grain boundaries) in the magnitude of 0.5–3 μm.

At high temperatures, although amphoteric and comparatively stable to both acid and basic slags and glasses, stabilised zirconia can be destabilised on prolonged contact with siliceous and alumino silicate compounds. The destabilisation of MgO partial stabilised zirconia is by the presence of SiO_2, TiO_2, Fe_2O_3 and Al_2O_3 enhanced, whereby SiO_2 dominates by removing the MgO of the zirconia crystal and producing magnesium silicates at the grain boundaries.[26]

In a previous work the corrosion mechanisms of low porous Mg–PSZ materials in steel/slag- systems have been extensively described by the aid of a corrosion testing device simulating operating conditions of submerged nozzles including the oscillation of the mould and the relative movement of the steel and the slag against the ceramic component.[27] The same device has been used for the corrosion evaluation of the present materials. The main task of this work is to improve the thermal shock behaviour of zirconia based materials by

keeping the corrosion resistance at least at the same level as in pure zirconia.

2. Experimental methods

The slip casting technique has been selected as the most suitable processing to disperse and incorporate homogeneously in the MgO partial stabilised zirconia matrix additional phases. Furthermore this forming process enables the manufacturing of thin wall components that are needed for near net shape casting technologies.[28]

A partial stabilised ZrO_2 (3.5 wt% MgO)-powder (Unitec, M3.5) with a grain size distribution of 0–12 μm and $d_{50} = 7.6$ μm has been used as the main component. A higher densification was achieved by a zirconia powder of $d_{50} = 2$–3.5 μm. The grain size distribution of 0–12 μm has remained.

There have been mixed different zirconia based slips of 70 wt% solids with 0.3 wt% electrolyte (related to solids); TiO_2 (Bayer, Bayertitan-T) of $d_{50} = 0.2$ μm, Al_2O_3 (Martinswerk, CS400) of $d_{50} = 2$ μm and $MgAl_2O_4$ (Alcoa, AR78) of $d_{50} = 3$–4 μm have been homogeneously dispersed in different compositions as listed in Table 1.

Discs of 100×4 mm have been slip casted and sintered at 1600°C in an electrical furnace by sintering curves obtained due to dilatometer curves. The obtained microstructures have been characterised by scanning electron microscope (SEM) and electron dispersive X-ray (EDX) analysis. Due to X-ray diffraction (XRD)[29,30] the zirconia phase composition (monoclinic, tetragonal and cubic) of the different materials has been measured. Further the monoclinic and tetragonal phase have been identified by transmission electron microscope (TEM) X-ray diffraction patterns.

The density and porosity of sintered samples were measured by Archimedes principle and in each case 20 samples for four point bending strength tests were cut out of discs and prepared according to the european norm EN 843 as fired. Strengths were measured at room temperature, at 1400°C and remaining strengths after quenching in water from 600 and 1000°C. Beside this thermal shock test, discs have been shocked thermally by an arc torch. In a further step the thermal expansion, the young modulus due to a grindo sonic frequency equipment and the thermal conductivity due to a laser flash system have been measured at elevated temperatures up to 1450°C. In addition the fracture toughness has been determined due to the hardness indentation technique.[31]

The characterisation has been completed through corrosion tests that have taken place in the special designed device as mentioned before. Specimens of 90×25×4 mm have been cut out of discs and placed in ceramic dyes based on MgO partial stabilised dense zirconia with 600 g steel St37 and 300 g slag (30 wt% SiO_2, 30 wt% CaO, 10 wt% Al_2O_3, 5 wt% F^-, 6–8 wt% Na_2O–K_2O, 10–12 wt% C_{total}) at 1550°C. The rotation (60 rotations through 90°/min) and the oscillation (lift10 mm, 60 oscillations/min) of the testing device have been tuned according to the conditions observed for conventional submerged nozzles during operation in steel plants.

3. Results and discussion

According to Table 1 the materials III and IV achieved less open pores than the pure zirconia material II.

In Table 2 the results of the XRD measurements are listed. Both pure materials I and II exhibit approximately the same amount of monoclinic, tetragonal and cubic phase. Through the addition of TiO_2 and Al_2O_3 (material III) approximately the whole amount of the tetragonal phase has been transformed and the monoclinic phase has increased tremendously. The XRD analysis identified spinel ($MgAl_2O_4$) and no free Al_2O_3 or TiO_2. It is assumed that TiO_2 has been incorporated in the zirconia lattice and a part of the MgO stabilising agent has been removed from the zirconia cell and has reacted with the Al_2O_3 to give $MgAl_2O_4$. Through the loss of the stabilising agent martensitic phase transformation occurred. The Ti^{4+} cations, as mentioned in the introduction, were not randomly incorporated in the lattice but in preferred energetic sites which caused a repulsion between the dopant cations and the vacancies. The removal of the Mg^{2+} out of the lattice was followed by

Table 1
Porosities

No.	Material (wt%)	Grain size of ZrO_2 d_{50} before firing (μm)	Open porosity (%)	Total porosity (%)
I	100% MgO (3.5 wt%) partial stab. ZrO_2	2–4	2	6
II	100% MgO (3.5 wt%) partial stab. ZrO_2	7–9	15	18
III	98% MgO (3.5 wt%) partial stab. ZrO_2, 1% TiO_2, 1% Al_2O_3	7–9	13	16
IV	98% MgO (3.5 wt%) partial stab. ZrO_2, 1% TiO_2, 1% $MgAl_2O_4$	7–9	14	16

Table 2
Zirconia phase composition

(Vol%)	Monoclinic	Tetragonal	Cubic
Material I pure zirconia	9.3	44.3	46.4
Material II pure zirconia	12.5	43.4	44
Material III with 1 wt% TiO_2, 1 wt% Al_2O_3	54.7	7.9	37.4
Material IV with 1 wt% TiO_2, 1 wt% $MgAl_2O_4$	13.2	52.3	34.5

the energetically suitable formation of spinel with the free alumina. The Ti^{4+} cations did not stabilise the zirconia.

Through the addition of $MgAl_2O_4$ instead of Al_2O_3 (material IV) no significant change of the monoclinic phase amount was observed. In this case no free MgO could be identified at the grain boundaries through EDX and XRD analysis and also the primary spinel has remained with the same amount of MgO (78 wt% Al_2O_3 and 22 wt% MgO). Further the material IV exhibit an increased amount of tetragonal precipitates. It is assumed that mechanical stress transformation of the cubic to the tetragonal phase occurred due to the spinel dispersed phase (lower thermal expansion coefficient than the cubic zirconia).

In Fig. 1 a surface (not polished) of material I is presented. Tetragonal precipitates of 1 μm and microporosity of 2–5 μm appear in 5–15 μm cubic grains and at their grain boundaries. In a higher magnification (Fig. 2) a nanoporous microstructure of the cubic phase can be observed. Similar tetragonal precipitates can be identified on the surface of material II but the micropores reach higher values, up to 10 μm. Material III is shown in Figs. 3–5. The tetragonal phase disappears and long sharp monoclinic twins are recognised and identified also by TEM X-ray diffraction patterns. During TEM sample preparation, in some crystals, tetragonal to monoclinic phase transformation occurred due to stresses resulting from ion thinning and electron beam heating. Further spinel phase is identified and the micropores of 10 μm disappear. In Figs. 6 and 7 microcracks are recognised, starting in the region of the spinel phase and diverting at the monoclinic grains. When free alumina and magnesia are present together in a mix and heated, spinel formation occurs, causing a 5% volume expansion.[32] This reaction starts approximately at 1000°C and is responsible for the microcrack formation of the material properties. Especially the thermal expansion coefficient and the young modulus are influenced strongly as it will be shown later.

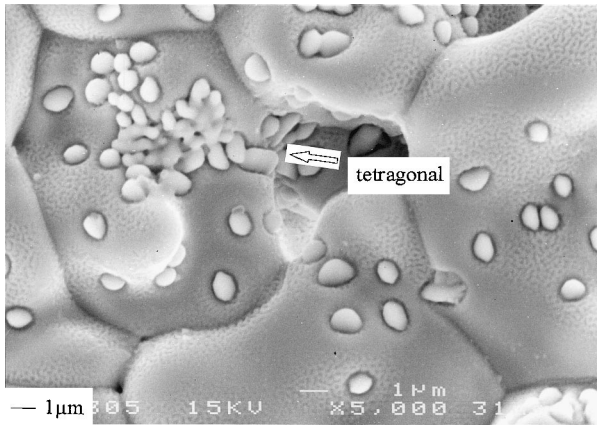

Fig. 2. Material I with nanoporosity, SEM micrograph (secondary electrons), cubic grains (12–15μm) and tetragonal in the magnitude of 0.5–1 μm.

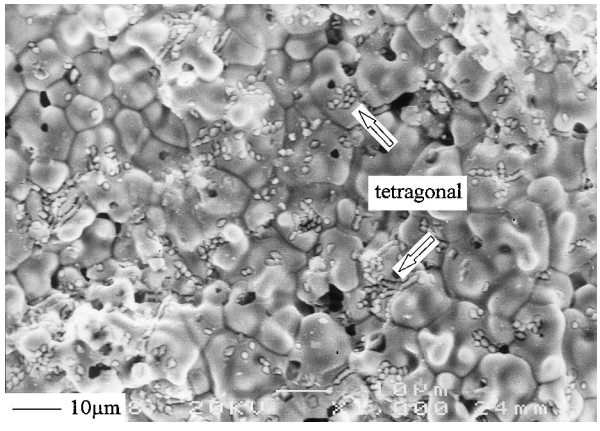

Fig. 1. Surface of material I, pure zirconia, SEM micrograph (secondary electrons).

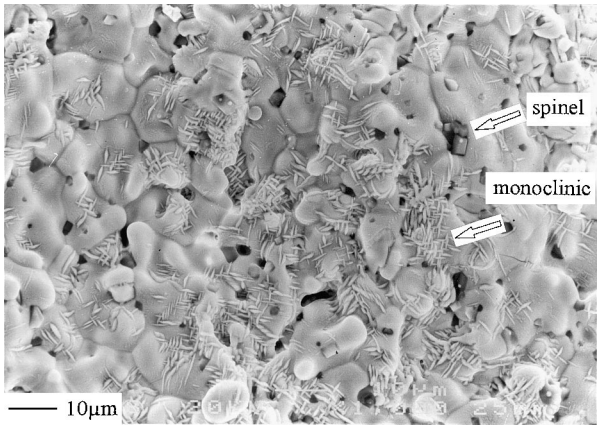

Fig. 3. Surface of material III, zirconia with additions, SEM micrograph (secondary electrons), long sharp monoclinic grains, cubic grains and spinel phase (black).

As discussed before no significant change of the monoclinic phase has been identified in material IV in comparison to I and II, Fig. 8. Tetragonal precipitates and spinel phase are observed in the cubic grains or at their boundaries. Apart from some individual tetragonal grains, the tetragonal phase appears more concentrated in groups of 20–40 precipitates in the cubic grains, Fig. 9.

According to the material properties (Table 3) material III reaches, at 1450°C, a thermal expansion coefficient of 5.5 10^{-6} K^{-1}, approximately 50% reduced compared to the pure zirconia materials. Considering the remaining strengths of the thermal shocked specimens materials III and IV exhibit a very good thermal shock performance at a ΔT of 600°C in comparison to the pure materials I and II. In addition the fracture toughness of materials III and IV consisting of zirconia and spinel has been enhanced.

In spite the fact, that with material III the lowest thermal expansion coefficient and young modulus of elasticity and in addition the highest remaining strengths were obtained, only material IV has survived a thermal shock attack due to an arc torch. In Figs. 10 and 11 discs of material III and IV are presented after

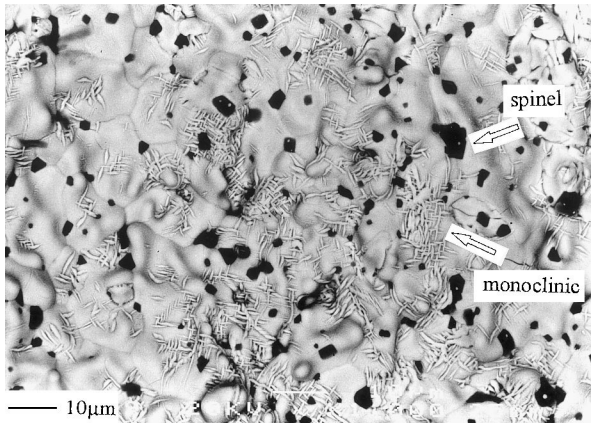

Fig. 4. Surface of material III, zirconia with additions, SEM micrograph (back scattering electrons), long sharp monoclinic grains, cubic grains and spinel phase (black).

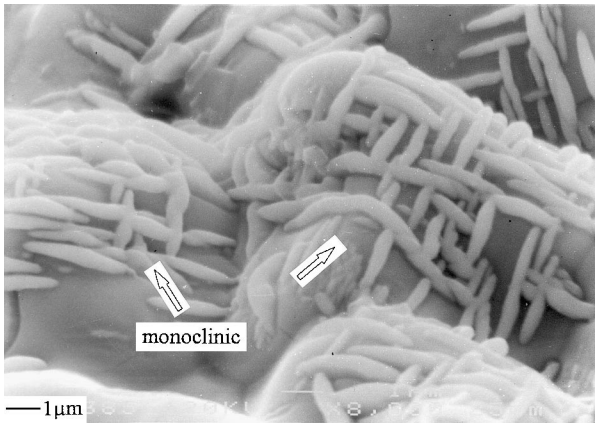

Fig. 5. Magnification of the surface of material III, long monoclinic twins in the cubic grains and at their boundaries.

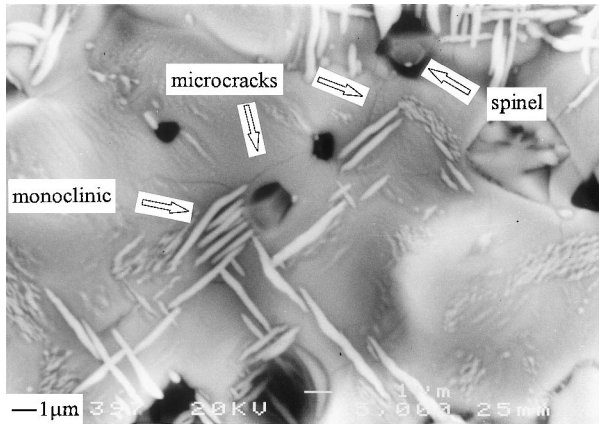

Fig. 6. Microcracks starting in the region of the spinel phase and diverted at the monoclinic twins.

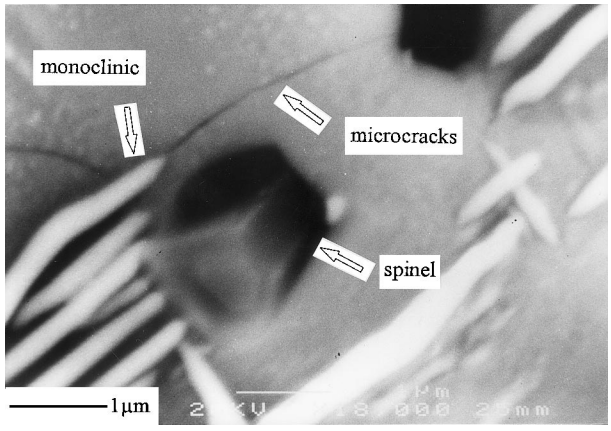

Fig. 7. Magnification of microcrack that has been diverted at the monoclinic phase.

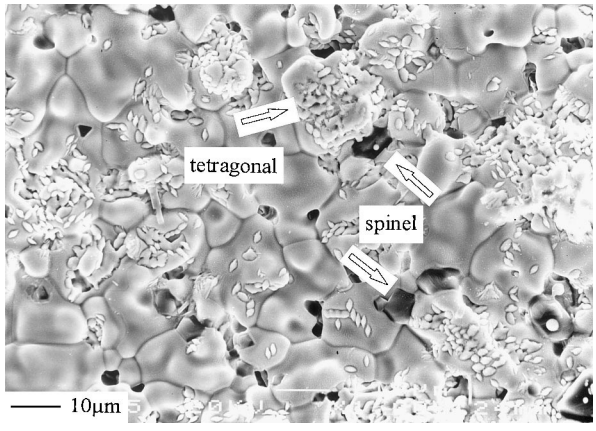

Fig. 8. Surface of material IV, zirconia with additions, SEM migrograph (secondary electrons), cubic and tetragonal zirconia grains with dispersed spinel phase.

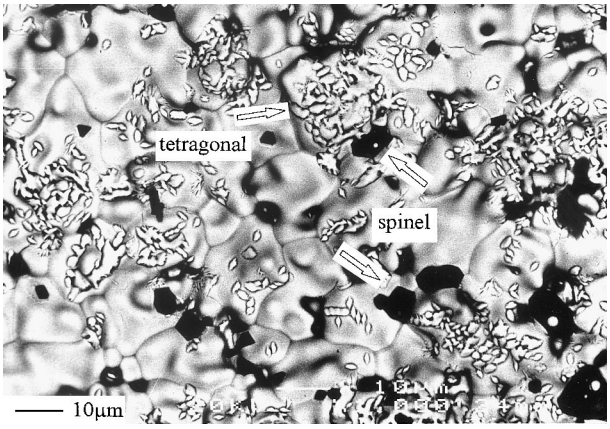

Fig. 9. Surface of material IV, SEM micrograph (back scattering electrons), spinel phase (black), groups of tetragonal precipitates and cubic grains.

Table 3
Material properties up to 1450°C

Properties		Material I	Material II	Material III	Material IV
σ_{RT}	MPa	177	164	138	163
$\sigma_{1400°C}$	MPa	55	35	54	56
K_{IC}	MPa $m^{1/2}$	4.5	4.0	6.5	5.5
$\sigma s_{600\ remaining}$	MPa	24	28	72	49
$\sigma_{1000\ remaining}$	MPa	13	16	46	42
E_{RT}	GPa	105	100	110	90
$E_{1000°C}$	GPa	90	75	60	65
$E_{1450°C}$	GPa	85	70	58	64
$\alpha_{600°C}$	10^{-6} /K	10.2	10	7.4	9.2
$\alpha_{1000°C}$	10^{-6} /K	10.7	10.5	6.6	8.5
$\alpha_{1450°C}$	10^{-6} /K	10.5	10.4	5.5	9.1
$\lambda_{600°C}$	W/m K	2.5	2.4	2.2	2.2
$\lambda_{1000°C}$	W/m K	2.5	2.3	2.1	2.2
$\lambda_{1450°C}$	W/m K	2.4	2.2	2.1	2.1

such a thermal shock attack. Material III failed after 90 s when a ΔT of 800°C (measured by thermocouples placed in the body of the discs) between the hot centre (spot of arc torch) and the outer area was achieved. In material IV microcracks are identified after the thermal shock attack, Fig. 12. These microcracks are observed at the spinel regions and are diverted at the tetragonal precipitates. This diversion caused martensitic phase transformation and the formation of monoclinic twins. A theory for stress induced tetragonal to monoclinic transformation of constrained zirconia is based on the assumption that when forcibly strained to a regime of absolute instability where the free energy density of the tetragonal phase has a negative curvature, the constrained tetragonal zirconia becomes unstable with respect to the development of a modulated strain pattern that will evolve into a band of twinned monoclinic domains.[33]

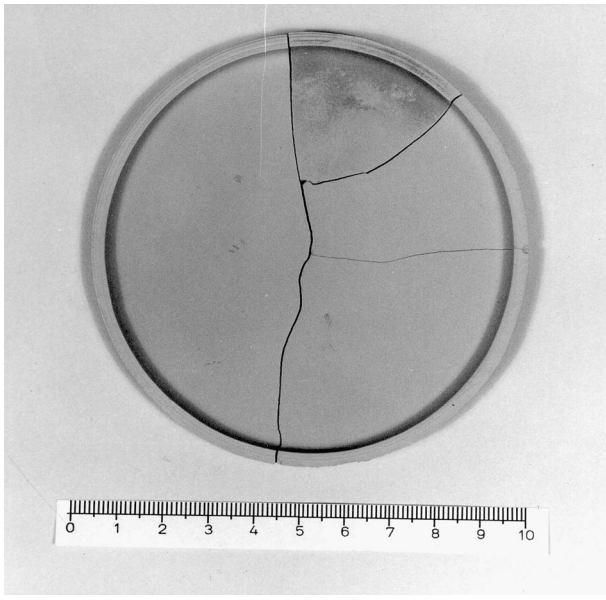

Fig. 10. Disc of material III after thermal shock attack (90 s) by an arc torch.

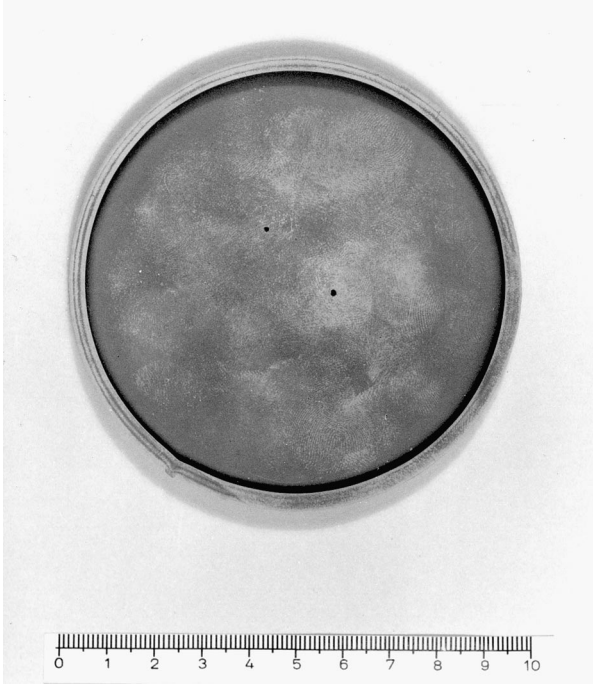

Fig. 11. Disc of material IV after thermal shock attack (5 min) by an arc torch.

Both materials contain spinel as secondary phase, probably also as a diversion phase. The energy of the thermal shock cracks is muffled in material IV due to the martensitic phase transformation of tetragonal to monoclinic and in material III due to the existing microcracks (caused by the spinel formation and by the martensitic phase transformation) and the diversion at the monoclinic grains. At temperatures above the

transformation temperature tetragonal to monoclinic the thermal shock resistance of material IV is impaired. The microcracks of material III caused by the martensitic phase transformation are cured partially but the microcracks caused by the spinel reaction remain and contribute to the thermal shock resistance at high temperatures (> 1200°C).

The thermal shock test of the remaining strengths exercised on four point bending strength specimens and the calculation of R_1 or R_2 thermal shock parameters as they are described by Hasselman, do not completely cover the thermal shock attack by an arc torch. In the case of the thermal shocked four point bending strength specimens a homogeneous heating and cooling over the surface is applied and thermal gradients are observed only across the depth. On the other hand the thermal shocked disc shapes by an arc torch present strong thermal gradients over the surface during heating and cooling down. Further, in case of the calculation of R_1 and R_2 parameters, the thermal expansion coefficient and the Young's modulus are considered as individual values measured at a specific temperature and no gradients are included. The thermal conductivity λ describes in R_2 how "easily" heat can be transferred, but again no gradients are enclosed.

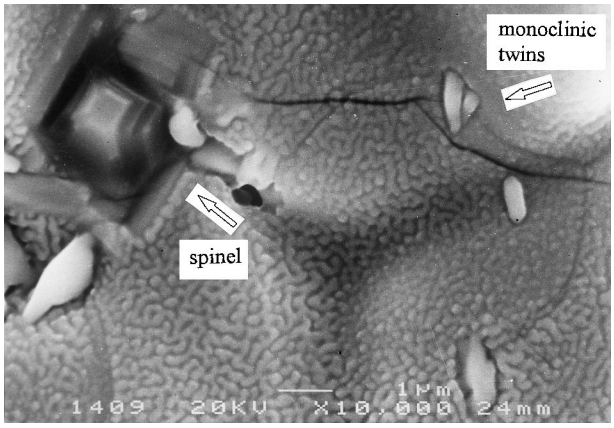

Fig. 12. Material IV, microcracks after thermal shock attack are diverted at the tetragonal precipitates followed by martensitic transformation of the tetragonal phase to monoclinic twins.

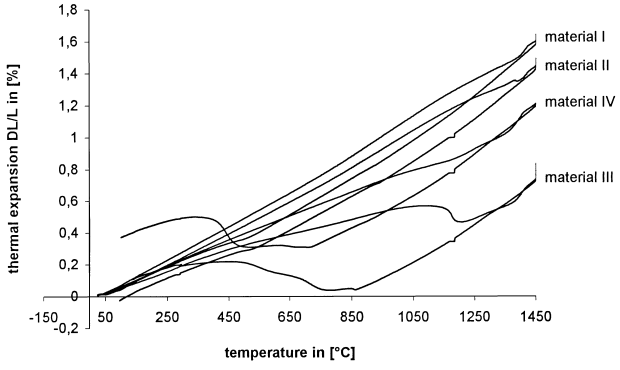

Fig. 13. Thermal expansion of different zirconia based materials up to 1450°C.

The thermomechanical behaviour of the microstructure at elevated temperatures depends on the matrix material, secondary phases, pores with different sizes and distributions, inclusions, phase transformations, heat treatments etc. and is registered mainly due to the thermal hysteresis. In Fig. 13 the thermal expansions during heating up and cooling down are listed. Material III exhibits a remarkable thermal hysteresis. At 900°C a thermal expansion coefficient of 5×10^{-6} K^{-1} is observed during heating up and at the same temperature during cooling down only a value 0.7×10^{-6} K^{-1} is measured. This difference is responsible for the failure of the disc based on material III. In spite of the higher values of the thermal expansion of material IV, the more linear behaviour of the thermal expansion accompanied by a higher amount of tetragonal metastable phase has led to a better thermal shock behaviour of the disc components.

In Table 4 the results of the corrosion tests are listed. The corrosion mechanisms have been already illustrated in another work.[27] Chemical destabilisation of the cubic and tetragonal grains occurs due to the diffusion of the Si and Na slag elements in the ZrO_2 cell. Si removes the MgO stabilising agent and settles at the grain boundaries as magnesium silicate. Due to the removal of the stabilising agent, martensitic phase transformation takes place followed by volume expansion and microcracks. The microstructure loses its integrity and new paths for slag penetration are created. Material III presents the highest corrosion resistance at the interfaces ceramic/steel/slag and ceramic/air/slag in comparison to

Table 4
Corrosion rates of zirconia based materials at the three main corrosive regions

Corrosion rate (mm/h) 2 h at 1550°C in steel/slag bath	Region A interface, ceramic/steel/slag	Region B interface, ceramic/air/slag	Region C steel bath
Material I pure zirconia	0.20	0.10	–
Material II pure zirconia	0.60	0.40	–
Material III with 1% TiO_2, 1% Al_2O_3	0.30	0.20	–
Material IV with 1% TiO_2, 1% $MgAl_2O_4$	0.50	0.30	–

materials II and IV with approximately the same porosity. This improvement deals with the higher monoclinic amount of material III that cannot be destabilised.

4. Conclusions

By the slip casting technique, zirconia dispersed materials have been developed with improved thermal shock and corrosion resistance performance.

In spite the fact, that in both materials III and IV only zirconia and spinel can be identified due to XRD and EDX quantitative analysis, their thermomechanical properties are different. Material III consists of secondary spinel, formed during sintering of the reaction between free alumina and the removed (from the zirconia lattice) magnesia. This reaction is followed by a 5% volume expansion and the formation of microcracks. In addition, due to the loss of the stabilising agent, martensitic phase transformation occurs followed again by microcrack formation. The sum of the microcracks is responsible for the reduction of the thermal expansion coefficient in comparison to pure materials (approximately 50%).

Material IV contains primary spinel and a much higher amount of tetragonal phase because of the fact that no stabilising agent has been removed from the zirconia cell. Further, the amount of the cubic phase has been decreased, probably due to mechanical stress transformation because of the spinel inclusions.[34] Material III exhibits a very good thermal shock performance according to the water quenching tests because of the lowest thermal expansion coefficient and Young's modulus of elasticity. Further its microstructure consists of microcracks due to the spinel formation that remain also at high temperatures above 1200°C. On the other hand material IV with the modified thermal expansion coefficient (higher than that of material III) presents the best results of thermal shocked disc shapes by an arc torch. Material III has failed because of the highest thermal hysteresis. The thermal shock conditions of the application have to be studied very carefully before choosing the best available modification or a combination of both of them. In the literature, in order to achieve a zirconia based material with a good thermal shock performance at least an amount of 30 vol% monoclinic phase has been suggested.[26] This composition offers a low thermal shock coefficient accompanied by an acceptable thermal hysteresis.

Zirconia materials with high amounts of monoclinic phase (above 50 vol%) present high porosity levels followed by worse corrosion resistance and pour mechanical strengths. In this matter material III is produced due to an in situ phase transformation with approximately 55% monoclinic phase, porosity less than 18%, a very good corrosion resistance against steel/slag-systems and four point bending strengths at RT above 120 MPa. The microcracks that are caused due to the zirconia destabilisation are muffled by the microcracks out of the spinel formation. Both microcrack patterns are overlapped and lead to sufficient mechanical strengths at RT.

The thermal hysteresis registers the influence of pores, inclusions, secondary phases, heat treatments etc. The R_1 and R_2 thermal shock parameters have to be modified and include also this information (of the hysteresis curve) due to a definition of a linearity factor related to the maximum difference of the thermal expansion at the same temperature during heating up and cooling down.

The $MgO–Al_2O_3$ binary system opens for the Mg–PSZ based materials the horizon of tailoring their thermomechanical properties for applications in near net shape steel processings through toughening mechanisms, whereby the amount of TiO_2 addition can control the rate of the formation of $MgAl_2O_4$ and the stabilising level.

Last but not least the ionic and electronic conductivity of materials III and IV have to be studied according to the contribution of $MgAl_2O_4$ defect structures and the TiO_2 semiconductor properties to new oxygen sensor approaches.

References

1. Stevens, R., *An Introduction to Zirconia*. Magnesia Electron publication Shervin Rivers Ltd, England, No. 113, 1983.
2. Leistner, H., Ratcliffe, D. and Schuler, A. Improved material design devices for continuous casting components. In *Proceedings of 2nd Worldwide Conference on Refractories*, Aachen, 1991, pp. 316–319.
3. Aneziris, C. G., Pfaff, E. M. and Maier, H. R., Ceramic materials in the system $ZrO_2–TiO_2–Al_2O_3$ for applications in the ferrous and non ferrous metallurgy, 5th Euro-Ceramics France. *Key Engineering Materials*, 1997, **3**(132–136), 1829–1833.
4. Parbel, W., Schruff, F., Bergmann, B. and Weiler, M. High quality refractory materials — the key to modern continuous casting technology. In *Proceedings of 44th Internat. Conference for Continuous Casting Brussel*, 1988, pp. 483–494.
5. Aneziris, C. G., Pfaff, E. M. and Maier, H. R., Designing principles of $ZrO_2–TiO_2–Al_2O_3–MgO$ based ceramics for refractory applications in the ferrous and nonferrous metallurgy. *3rd International Refractory Congress IREFCON 98 Calcutta India*, 1998, **2**, 339–344.
6. Hasselman, D. P. H., Thermal stress resistance parameters for brittle refractory ceramics. *Ceramic Bulletin*, 1970, **49**(12), 1033–1037.
7. Hasselman, D. P. H., Unified theory of thermal shock fracture initiation, crack propagation in brittle ceramics. *J. Am. Ceram. Soc.*, 1969, **52**(11), 600–604.
8. Stubican, V. S., Phase equilibria and metastabilities in the system $ZrO_2–MgO$, $ZrO_2–CaO$ and $ZrO_2–Y_2O_3$. In *Science and Technology of Zirconia III*, USA, Westerville OH, 1986, pp. 71–82.
9. Evans, P., Stevens, R. and Binner, J. G. P., Quantitative X-ray diffraction analysis of polymorphic mixes of pure zirconia. *Br. Ceram. Trans. J.*, 1984, **83**, 39–43.

10. Hannink, R. H. J. and Garvie, R. C., Sub-eutectoid aged Mg–PSZ alloy with enhanced thermal up-shock resistance. *J. Mat. Sci.*, 1982, **17**, 2637–2643.
11. Duan, K., Wing Mai, Y. and Cotterell, B., Resistance to crack propagation in an Al_2O_3/ZrO_2 Ceramic. In *Science and Technology of Zirconia V*. Technomic Publishing Co., Pennsylvania, USA, 1993, pp. 482–492.
12. Mchale, A. E. and Roth, R. R., Low temperature phase relationships in the system ZrO_2–TiO_2. *J. Am. Ceram. Soc.*, 1986, **69**(11), 827–832.
13. Khor, K. A. and McPherson, R., Formation of ultrafine multicomponent ZrO_2-based powders in an RF plasma. In *Science and Technology of Zirconia V*. Technomic Publishing Co., Pennsylvania, USA, 1993, pp. 215–222.
14. Kountouros, P. and Petzow, G., Defect chemistry, phase stability and properties of zirconia polycrystals. In *Science and Technology of Zirconia V*. Technomic Publishing Co., Pennsylvania, USA, 1993, pp. 30–48.
15. Lin, C. L., Gan, D. and Shen, P., The effects of TiO_2 addition on the microstructure and transformation of ZrO_2 with 3 and 6 mol% Y_2O_3. *Mat. Sci. Eng., A*, 1990, **129**, 147–155.
16. Yokokawa, H., Sakai, N., Kawada, T. and Dokiya, M., Phase diagram calculations for ZrO_2 based ceramics: thermodynamic regularities in zirconate formation and solubilities of transition metal oxides. In *Science and Technology of Zirconia V*. Technomic Publishing Co., Pennsylvania, USA, 1993, pp. 59–68.
17. Zschech, E., Kountouros, P. and Petzow, G., Synchrotron radiation Ti-K XANES study of TiO_2–Y_2O_3-stabilized tetragonal zirconia polycrystals. *J. Am. Ceram. Soc.*, 1993, **76**(1), 286–287.
18. Brown, F. H. and Duwez, P., The zirconia — titania system. *J. Am. Ceram. Soc.*, 1953, **37**(3), 129–133.
19. Arias, A., Thermal shock resistance of zirconia with 15 mol% titanium. *J. Am. Ceram. Soc.*, 1966, **49**(6), 334–338.
20. Arias, A., Mechanism by which metal additions improve the thermal shock resistance of zirconia. *J. Am. Ceram. Soc.*, 1996, **49**(6), 339–341.
21. Weber, B. C., Garnet, H. J., Mauer, F. A. and Schwartz, M. A., Observations of the stabilisation of zirconia. *J. Am. Ceram. Soc.*, 1956, **39**(6), 197–206.
22. Meschke, F., de Portu, G. and Clausen, N., Preparation and characterisation of fine-grained (Mg, Y)-PSZ ceramics with spinel additions. In *Science and Technology of Zirconia V*. Technomic Publishing Co., Pennsylvania, USA, 1993, pp. 378–385.
23. Grimm, N., Verbesserung von dichten Zirkondioxid-Werkstoffen für keramische Bauteile in Verschlußsystemen für den flüssigen Stahl. Dissertation thesis, Technical University of Aachen, 1993, pp. 82–115.
24. Kelly, P. M. and Ball, C. J., Crystallography of stress induced martensitic transformation in partially stabilised zirconia. *J. Am. Ceram. Soc.*, 1986, **69**(3), 259–264.
25. Behrens, G., Martinez-Fernandez, J., Dranswaan, G. W. and Heuer, A. H., Isothermal martensitic transformation in ZrO_2 ceramics. In *Science and Technology of Zirconia V*. Technomic Publishing Co., Pennsylvania, USA, 1993, pp. 3–15.
26. Endres, H. G., Einfluß des Sinterverhaltens und der Gefügeausbildung auf das Ausdehnugs- und Thermoschock-verhalten von ZrO_2-Werkstoffen. Dissertation thesis. Technical University of Aachen, 1985, pp. 18–70.
27. Aneziris, C. G., Pfaff, E. M. and Maier, H. R., Corrosion mechanisms of low porosity ZrO_2 based materials during near net shape steel casting. *J. Eur. Ceram. Soc.*, 2000, **20**(2), 159–168.
28. Aneziris, C. G., Bauteile bestechen durch schlanke Linie. In *Industrieanzeiger*, special edition. *Technical Ceramics*, 5, 1998, pp. 56–57.
29. Diaz, M. J. and Edirisinghe, R. B., Characterisation of a zirconia–yttria–titania thermal barrier coating. *J. Mat. Sci. Lett.*, 1994, **13**, 1595–1598.
30. Iwamoto, N. and Umesaki, E. S., Characterisation of plasma-sprayed zirconia coatings by X-ray diffraction and Raman spectroscopy. *Thin Solid Films*, 1985, **127**, 129–137.
31. Nihara, K., Morena, R. and Hasselman, D. P. H., Indentation fracture toughness of brittle materials for palmqvist cracks. *Fracture Mechanics of Ceramics*, 1983, **5**, 97–105.
32. Carbone, T. J., Characterisation and refractory properties of magnesium spinel raw materials. *Proceedings of XXVII Intern. Refractory Congress in Aachen*, Germany, 1984, pp. 523–554.
33. Chan, S. K., Nucleation in stress-induced tetragonal–monoclinic transformation of constrained zirconia. In *Science and Technology of Zirconia V*. Technomic Publishing Co., Pennsylvania, USA, 1993, pp. 16–29.
34. Sakuma, T., The cubic to tetragonal transformation in zirconia alloys. In *Science and Technology of Zirconia V*. Technomic Publishing Co., Pennsylvania, USA, 1993, pp. 86–98.